The Morphological Evolution of Dendritic Microstructures during Coarsening

R. MENDOZA, J. ALKEMPER, and P.W. VOORHEES

The coarsening process in systems consisting of spherical particles in a matrix has been studied extensively. In contrast, coarsening in systems that possess both positive and negative curvature, such as those present following dendritic solidification, have received less study. Recent advances in experimental technology now allow for the routine analysis of metallic microstructures in three dimensions. A method has also been developed to determine the mean and Gaussian interfacial curvature, the analogs of the particle size distribution for spherical particles. The evolution of dendritic microstructures during coarsening is analyzed for a directionally solidified Al-15 wt pct Cu alloy. Samples were taken from this ingot and isothermally coarsened for 10 and 964 minutes. Probability density plots of the mean and Gaussian curvature as well as probability density plots of the principal curvatures show that extreme positive and negative mean curvatures decrease, that most of the interfaces are saddle-shaped, and that solid spherical shapes disappear to a greater degree than liquid spherical shapes. Probability density plots of the orientation of the surface normals within the microstructure show that the majority of the interfaces are parallel to the growth direction and that there is a fourfold symmetry in the 10-minute sample and a twofold symmetry in the 964-minute sample.

I. INTRODUCTION

A MUSHY zone, a mixture of liquid and dendrites, commonly forms during solidification. It is well known that the overall properties of a solidified metal are determined by the evolution of this dendritic solid-liquid mixture. Thus, understanding the evolution of this structure is critical in quantifying the link between the properties of the solidified ingot and its processing history.

Soon after formation, the dendritic morphologies in the mush are altered through a coarsening or Ostwald ripening process. Under isothermal conditions, coarsening occurs since the composition in the liquid at the interface is a function of the mean curvature of the solid-liquid interface as expressed by the Gibbs–Thomson equation for a binary alloy:

$$C = C_\infty + l_c H \qquad [1]$$

where C is the composition in the liquid at the solid-liquid interface, C_∞ is the equilibrium composition of the liquid at a flat interface, l_c is the capillary length that is a function of the solid-liquid interfacial energy, and H is the mean curvature of the interface equal to $(1/R_1 + 1/R_2)/2$, with R_1 and R_2 being the principal radii of curvature. Therefore, interfacial areas with different curvatures will have different liquid compositions, leading to fluxes of solute and the evolution of the morphology of the solid-liquid mixture. During this process, the total interfacial area, and with it the total interfacial energy, decreases.

Figure 1(a) shows a freely grown dendrite and Figure 1(b) shows the mean curvature of the interfaces. The curvature variations and the corresponding matrix concentration variations lead to fluxes of solute from high mean curvature regions to low mean curvature regions. The interface moves due to the fluxes and the dendrite coarsens. As the mean interfacial curvature is responsible for these solute fluxes, to fully understand the coarsening process, characterization of the interface curvature as a function of time during coarsening is necessary.

In contrast to dendritic solid-liquid mixtures, the coarsening process in a two-phase system with a distribution of spherical particles of various radii, R, is relatively well understood. Since the mean curvature of a sphere is given by $H = 1/R$, the concentration at the surface of small particles will be higher than that for large particles; thus, over time, the radii of the small particles will decrease while the radii of large particles will increase. Throughout these changes, the total volume fraction of solid remains nearly constant. The average particle size, $\overline{R}$, increases with time, while the number density of particles decreases. The total interfacial area, and hence total interfacial energy, decreases as the number density of particles decreases. A particularly important aspect of the coarsening process of a system of spherical particles is that the composition along the interface of a spherical particle is constant, because the curvature of a spherical particle is constant. Thus, a single parameter, the particle radius, sets the interfacial concentration. This permits analytical theories for the coarsening process to be developed. In contrast, the curvature at a point on a dendrite is not solely a function of the size of a dendrite and the curvature varies with position along the interface. Furthermore, unlike dendritic solid-liquid mixtures, for systems of spherical particles it is only necessary to measure the particle radius distribution and the spatial distribution of the particles to determine the diffusion field and, hence, the coarsening kinetics.

Another important characteristic of the coarsening process, or Ostwald ripening, of a system of spherical particles

R. MENDOZA, Graduate Research Assistant, J. ALKEMPER, Assistant Professor, and P.W. VOORHEES, Professor, are with the Department of Materials Science and Engineering, Northwestern University, Evanston, IL 60208-3108. Contact e-mail: r-mendoza@northwestern.edu

This article is based on a presentation given in the symposium "Fundamentals of Solidification" which occurred at the TMS Fall meeting in Indianapolis, Indiana, November 4-8, 2001, under the auspices of the TMS Solidification Committee.

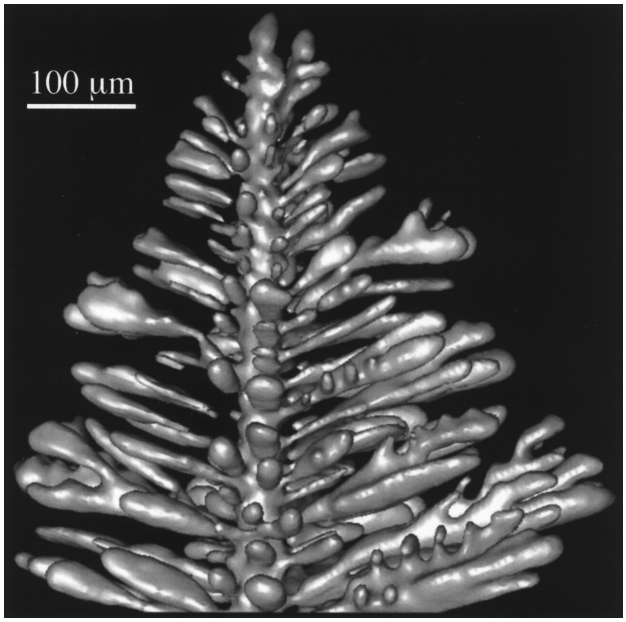

(*a*)

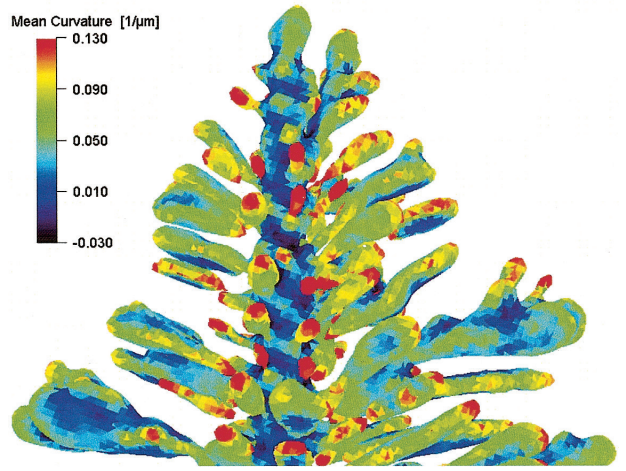

(*b*)

Fig. 1—(*a*) Three-dimensional reconstruction of a free-growing aluminum dendrite in an aluminum-copper eutectic liquid. Solid denotes the aluminum dendrite while the eutectic phase was omitted for viewing clarity. (*b*) The mean interfacial curvature is shown for the top portion of (a).

is self-similarity. Originally proposed by Lifshitz and Slyozov[1] and Wagner[2] for infinitely separated, spherical particles, it was predicted that after a long period of time, the microstructure becomes self-similar when scaled by the time-dependent length scale, *e.g.*, $\overline{R}$, where $\overline{R}$ evolves as

$$\overline{R}^3\,(t) - \overline{R}^3\,(0) = K_{\mathrm{LSW}}\,t \qquad [2]$$

where $\overline{R}(t)$ is the average particle radius at a time t, $\overline{R}(0)$ is the average particle radius at the start of self-similar coarsening, and K_{LSW} is the coarsening constant. This also implies that the particle size distribution becomes time independent when scaled by $\overline{R}(t)$.

Since dendrites are clearly not spherical, there are many possible time-dependent length scales that can be employed to characterize the coarsening process. Much of the initial work on dendrite coarsening focused on measuring the secondary arm spacing of the dendrites, λ_2, because it increases

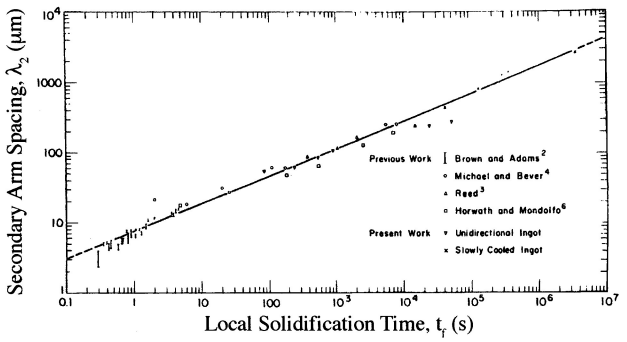

Fig. 2—Secondary arm spacing, λ_2, as a function of local solidification time, t_f, for Al-4.5 wt pct Cu.[3]

during coarsening in a similar fashion as the average particle size for a system of spherical particles and is easy to measure. The increase in λ_2 with time follows from the fact that those secondary arms that have spent more time suspended in the liquid than others will have more time to coarsen.

For a system that is continuously cooled, the increase in λ_2 should therefore correlate with the time required for a fixed location to go from the liquidus to the solidus temperature, the local solidification time, t_f. Figure 2 shows the dependence of secondary arm spacing on the local solidification time for the Al-4.5 wt pct Cu system. The increase in secondary dendrite arm spacing reflects an increase in the size scale of the system. Measurements of the local solidification time ranged from under 1 second to 10^7 seconds. Throughout this large range of t_f, $\lambda_2 \sim t_f^{1/3}$.

However, measuring λ_2 after significant morphological changes have occurred poses a serious problem. As an example, Marsh and Glicksman coarsened a Sn-40 pct Bi sample for long periods of time and showed that an initially dendritic microstructure can evolve to a system of spheroidal solid particles, for which a secondary arm spacing cannot be measured.[4] Another length scale that is independent of the morphology is therefore needed to characterize the coarsening process. One possibility is the inverse of the surface area per unit volume, $1/S_v$. In analogy to Eq. [2], the relationship between S_v and time is

$$S_v^{-3}\,(t) - S_v^{-3}\,(0) = Kt \qquad [3]$$

In the Marsh and Glicksman experiment, it was discovered that, even after the dramatic morphological changes from a dendritic mixture to one consisting of spheroidal particles had taken place, S_v was still linearly related to $t^{-1/3}$ (Figure 3).

Many models for the temporal evolution of λ_2 have been proposed. Despite the variation in curvature with position, as shown in Figure 1, the majority of models assume that the dendrite arms have a cylindrical shape. For example, Kattamis *et al.* considers the situation where all of the arms are cylindrical and one is thinner than the rest.[5] The matrix has a higher concentration at the interface of the thinner arms, as given by the Gibbs–Thomson Eq. [1], compared to the larger arms. This leads to a flux of solute from thinner to thicker arms resulting in the axial remelting of the thinner arm at a rate that is proportional to the difference in the radius of the dendrite arms.

Kahlweit also considers cylindrical dendrite arms, but assumes that they have a spherical tip.[6] Assuming this morphology, the mean curvature of the tip would be twice

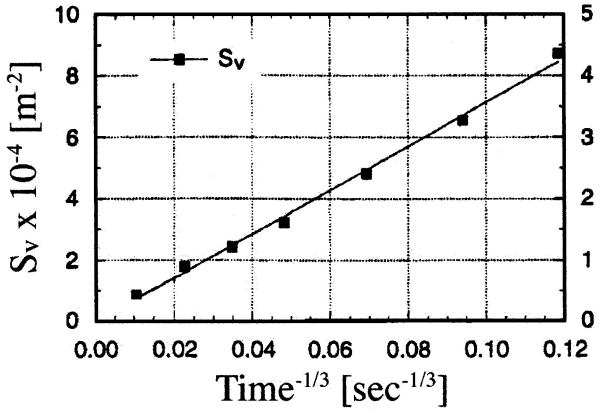

Fig. 3—Surface area per unit volume at different times for Sn-40 pct Bi.[4]

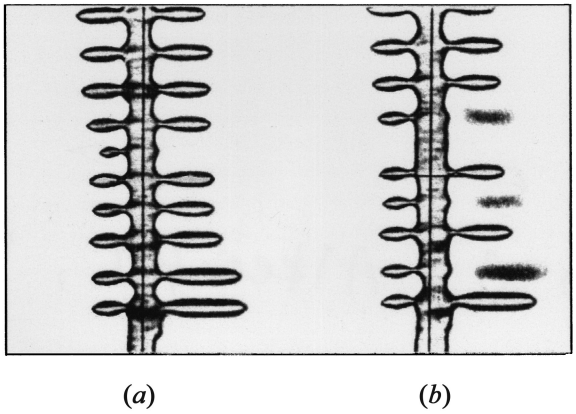

Fig. 5—Separation of dendrite arms in NH_4Cl: (*a*) $t = 18$ min and (*b*) $t = 32$ min.[7]

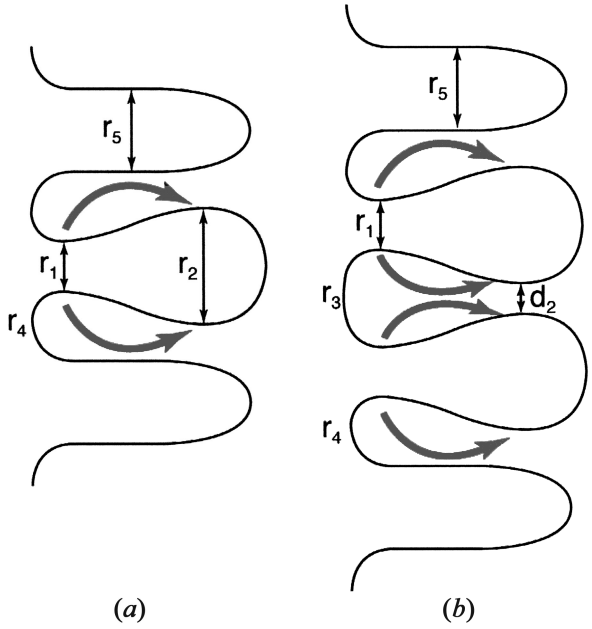

Fig. 4—Material transport for (*a*) one tear-shaped arm surrounded by cylindrical arms[8,9] and for (*b*) two tear-shaped arms surrounded by cylindrical arms.[10]. Gray arrows represent the direction of material transport.

the mean curvature of the cylindrical part of the dendrite arm. Material is transported away from the tip of a thinner dendrite arm, leading to axial remelting at a fixed rate that is again proportional to the radius of the arm. This process has been observed in experiments for some dendritic solid-liquid mixtures.[7]

The assumption that the dendritic arms are cylindrical is not generally valid (Figure 1). Dendrites are complex structures with curvature variations along the arms that determine how the arms will coarsen. Some models consider the dendrite arms to be tear-shaped.[8,9] They consider only the radius of curvature near the base, r_1, and the larger radius of curvature near the tip, r_2 (Figure 4(a)). Since $r_2 > r_1$, material is transported from the base to the region near the tip of the arm, thereby decreasing r_1 and increasing r_2. This process may continue until r_1 becomes zero and the tear-shaped arm detaches from the stem of the dendrite. Experimental evidence of this process is shown in Figure 5, where all of the NH_4Cl dendrite arms have a tear-shape morphology. Curvature differences lead to separation of the tear-shaped arms from the main branch. After separation, the detached arms move out of focus in Figure 5(b). This model, however, does not consider the saddle-shaped interfacial area between the tear-shaped arm, r_4. The saddle-shaped interfaces will have one negative radius of curvature, which is not considered by this model. Thus, while this model describes the mechanism responsible for secondary dendrite arm detachment, it is unlikely that the kinetics of the detachment process given by this model is accurate.

The interaction of two neighboring, tear-shaped dendrite arms has also been considered.[10] Figure 4(b) shows how material is transported away from the bases and accumulates at the cylindrical region near the tip, decreasing the distance between the two arms, d_2. The diameter of the arms near the tips continues to grow until the arms contact and form a single dendrite arm. Figure 6 shows the coalescence of dendrite arms *J* and *I* in two tear-shaped surfaces, r_3, or the saddle-shaped surfaces between the tear-shaped surfaces and the cylindrical arms, r_4. In examining Figure 6, one can see that material accumulates in the saddle-shaped area between the two arms *J* and *I*, growing closer toward the tip. The curvature of the neighboring cylindrical arms was also not considered in this model.

All of the models isolate and thus describe only parts of the coarsening process due to the complexity of morphology of a dendrite and its surroundings. They also demonstrate the importance of the actual shape of the dendrite arm and how its curvature influences the coarsening process. The greatest drawback of these models is the lack of quantitative experimental verification. Quantitative tests must inevitably involve the ability to track the surface curvature through the coarsening process. In addition, it is likely that in mushy zones the microstructure is sufficiently complex that theories based upon the evolution of a single dendrite secondary arm will not yield a predictive theory for the evolution of the solid-liquid mixture.

Experimentally, a morphology-independent measure of the microstructure during coarsening is required. It must allow for topological transitions such as arm coalescence, arm detachment, and the transition to spherical particles, as previously mentioned. The surface area per unit volume, S_v, allows for such transitions, while being morphology-independent, but it is only an average over the system and

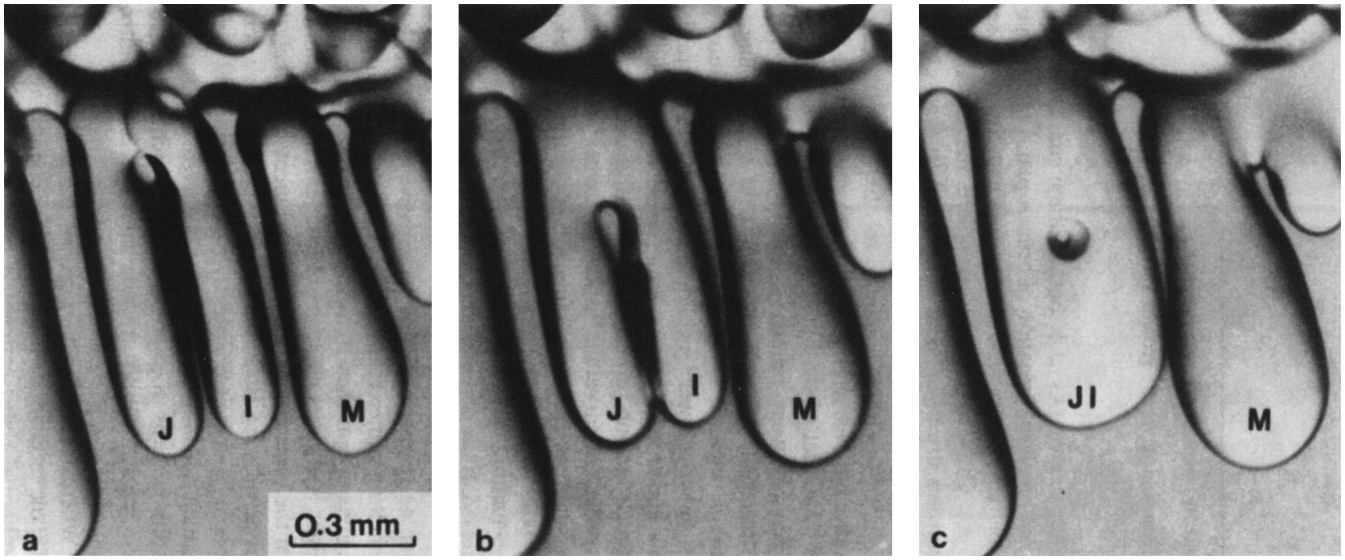

Fig. 6—(*a*) through (*c*) Coalescence of secondary arms *J* and *I*, in succinonitrile. Time between photographs is 20 to 30 min.[11]

cannot address the detailed evolution of regions of the microstructure. In order to measure these details, we have determined the evolution of interfacial curvature during coarsening. This method thus makes no *a priori* assumptions on the morphology of the microstructure and obtains directly the interfacial property that drives the coarsening process: the mean curvature of the solid-liquid interface as a function of position along the interface. Measurements of the mean and Gaussian interfacial curvature for a dendritic mixture provide the analogs of the particle size distribution of a system of spherical particles.

II. EXPERIMENTAL SETUP

A Bridgman-type furnace was used to directionally solidify a Al-15 wt pct Cu alloy rod. The furnace used differed from the typical Bridgman setup in that the rod was held stationary and was isolated from the moving furnace. This prevented vibrations from possibly affecting the solidification process. The rod was solidified using a temperature gradient of 3.33 K/mm and a growth velocity of 0.02 mm/s.

Samples taken from the directionally solidified rod were isothermally coarsened at 553 °C, 5 deg above the eutectic temperature, for 10 and 964 minutes. The coarsening was performed in a small furnace that was suspended inside a larger furnace. The larger furnace controlled the ambient temperature as the samples coarsened. This furnace-within-a-furnace design was employed to quickly achieve the coarsening temperature and, more importantly, to minimize the thermal gradients in the sample. The samples were then quenched, converting any liquid present during coarsening to eutectic solid.

A recently developed serial sectioning technique was used to obtain the coarsened microstructure in three dimensions.[12] Sections taken 4.75 μm apart were combined to form a three-dimensional image of the microstructure. Curvature information could then be extracted by the method described in Section III.

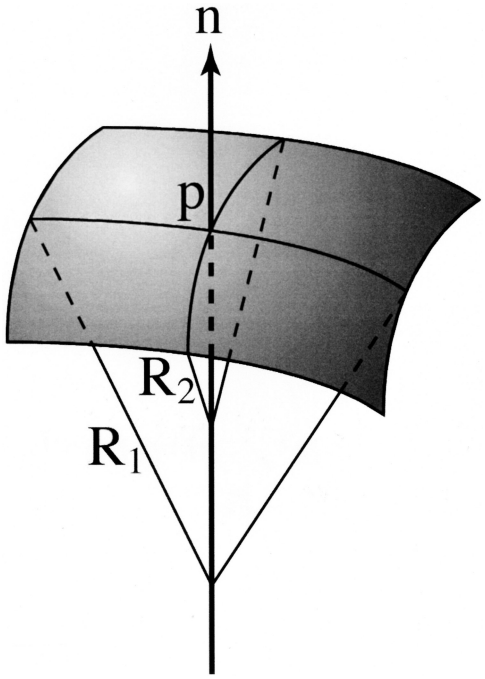

Fig. 7—Surface patch with its corresponding radii of curvature, R_1 and R_2, at a point of interest *p*. **n** is a unit vector that is perpendicular to the patch at *p*.

III. ANALYSIS

As mentioned in Section I, three-dimensional measurement of the interface curvature is necessary to fully characterize the coarsening process. A general surface can be described locally by a patch, similar to the one shown in Figure 7. The shape of the surface at point *p* at the center of the patch can be completely characterized by two principal radii of curvature, R_1 and R_2. Each radius corresponds to an imaginary circle that is tangent to the surface patch. These circles are perpendicular to each other and represent the maximum and minimum radii curvatures of the patch.

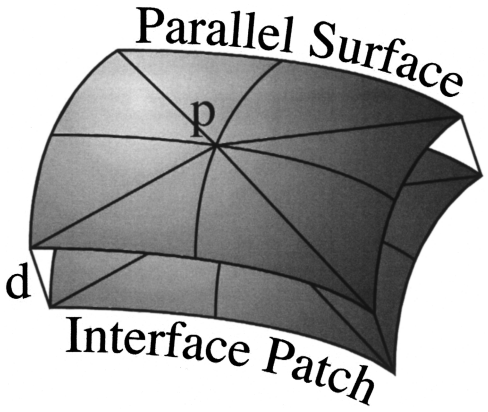

Fig. 8—Parallel surface constructed from surface patch.

Equivalently, two other parameters may be used to characterize the surface curvature, the mean curvature, H, and the Gaussian curvature, K, given by

$$H = \frac{1}{2}\left(\frac{1}{R_1} + \frac{1}{R_2}\right) \quad [4]$$

$$K = \left(\frac{1}{R_1 R_2}\right) \quad [5]$$

The mean curvature, H, determines the solute concentration at the interface according to the Gibbs–Thomson equation. This interfacial solute concentration serves as a boundary condition for the diffusion equation, a solution to which yields the local interfacial velocity. As material is deposited or removed, the mean curvature will change. This change also depends on the Gaussian curvature, because the evolution of the Gaussian and mean curvature are linked.[13] The importance of the Gaussian curvature is also illustrated by a saddle-shaped surface in which $R_1 = -R_2$. In this case, $H = 0$; thus, the interfacial solute concentration is equal to that of a planar interface, even though the interface is clearly not planar. It is necessary to measure both the mean and Gaussian curvatures in order to characterize the coarsening process.

The three-dimensional mean and Gaussian curvature information can be obtained using a method employed by Jinnai *et al.*[14] This involves triangulating the interface and constructing a parallel interface by displacing each surface point by a distance d normal to the interface, as shown in Figure 8. The area of the parallel interface, $A(d, p)$, is related to the area of the original interface patch, $A(0, p)$, by

$$A(d, p) = A(0, p)\,(1 + 2H(p)d + K(p)d^2) \quad [6]$$

By constructing a parallel interface at two different distances, one obtains two equations with two unknowns allowing one to solve for H and K at a point p and completely characterizing the surface shape at that point.

Once H and K have been determined for each interface point, it is possible to plot the curvature information of the analyzed microstructure, as shown in Figure 9. $P(H, K)$ is a probability density function such that $P(H, K)dHdK$ is the probability that, at a randomly chosen surface point, the mean curvature H to $H + dH$ and a Gaussian curvature K to $K + dK$. Figure 9 is the analogue to the particle size distribution of a system composed of spherical particles.

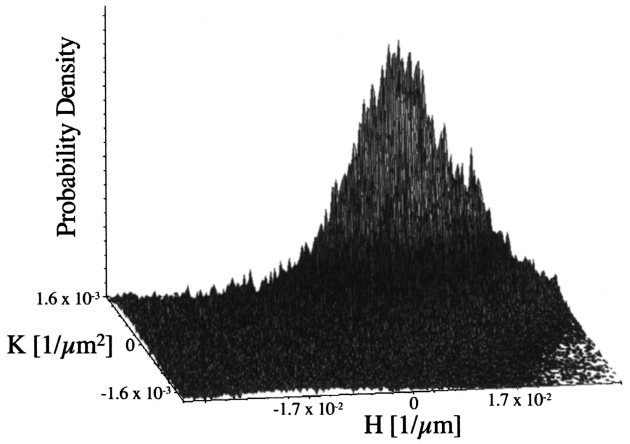

Fig. 9—Mean and Gaussian curvature probability plots for the sample coarsened for 10 min.

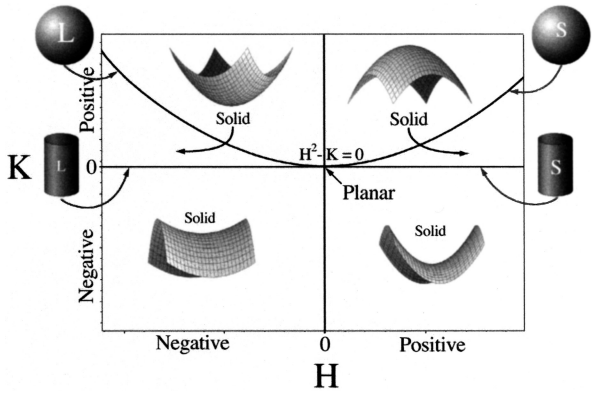

Fig. 10—Map of local interfacial shapes for the H–K contour plots. These are generated by looking down the z-axis of Fig. 9 and generating contours corresponding to a given height.

Data similar to Figure 9 were used by Alkemper and Voorhees[15] to generate two-dimensional plots that displayed H and K distributions independently. This method, however, made it impossible to examine the functional relationship between H and K. Since it is difficult to visualize the relationship between H and K using these two-dimensional plots, contour plots were generated from the three-dimensional probability density plots, such as Figure 9. This allows one to determine the most probable interfacial shapes within the microstructure (Figure 10). Solving for $1/R_1$ or $1/R_2$ in Eqs. [4] and [5], one obtains the relationship $H^2 - K \geq 0$. There can be no data in the area above the $H^2 - K = 0$ line in Figure 10. Curvatures that lie on the line correspond to spherical local interfacial shapes. If H is positive, the interface has a solid spherical shape, while if H is negative, it has a liquid spherical shape. If a point on the interface has a positive Gaussian curvature, the concavity of the interface is determined by the sign of H. If H is positive, the interface is concave toward the solid, while if H is negative, it is convex toward the solid. An interface with $K = 0$ has a cylindrical interface composed of solid (if H is positive) or liquid (if H is negative). Saddle-shaped interfaces are characterized by negative Gaussian curvatures. The sign of the mean curvature determines the dominant principal curvature. Important to note is that the chemical potential

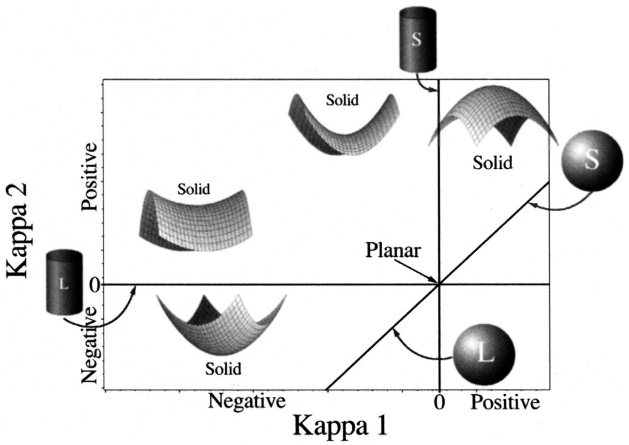

Fig. 11—Map of local interfacial shapes for the κ_1-κ_2 probability density plots.

is constant for a given H. Thus, it is possible for two different local interfacial shapes corresponding to different K to have the same chemical potentials. For example, all interfaces with $H = 0$ but $K \neq 0$ have the same chemical potential as a planar interface even though the interface patches are not planar.

An alternate way of presenting curvature information is by constructing probability density plots of κ_1 *vs* κ_2 defined as $(1/R_1)$ and $(1/R_2)$, respectively (Figure 11). A forbidden region is also found in this plot, located below the line $\kappa_1 = \kappa_2$. An interfacial shape on the $\kappa_1 = \kappa_2$ line corresponds to spherical shape. $\kappa_1 = \kappa_2 > 0$ indicates solid spherical shapes, while $\kappa_1 = \kappa_2 < 0$ indicates liquid spherical shapes. However, if $\kappa_1 = \kappa_2 = 0$, the interface is planar. Cylindrical shapes are characterized by $\kappa_1 = 0$ (solid cylindrical shapes) or $\kappa_2 = 0$ (liquid cylindrical shapes). Negative κ_2 indicates that the interface is convex toward the solid, while positive κ_2 is concave toward the solid. Surfaces with positive κ_2 and negative κ_1 are saddle-shaped.

The interfacial normals of the surface may also be used to determine if there is any preferential directionality in the microstructure. The orientation of the normal vectors, **n**, can be determined by obtaining ϕ and θ, where ϕ and θ are spherical coordinates of **n**. The value of ϕ varies between 0 and 2π, while θ varies from 0 to π. $\theta = 0$ corresponds to the growth direction. One can plot the probability density $P(\phi, \theta)$, where $P(\phi, \theta)d\phi d\theta$ is the probability that at a randomly chosen point the interface normal has an orientation between ϕ to $\phi + d\phi$ and θ to $\theta + d\theta$. To illustrate, if ϕ and θ were measured for a cylindrical microstructure that is parallel to the growth direction, all the normals (**n**) would be perpendicular to the growth direction and would be represented on the plot as a line along $\theta = \pi/2$.

IV. RESULTS AND DISCUSSION

Three-dimensional reconstructions of the microstructures for the 10- and 964-minute isothermally coarsened samples are shown in Figures 12 and 13, respectively. Analysis for each sample was done within a single grain. Both samples have a volume fraction of solid equal to 74 pct. It is evident by comparing the two samples that the microstructure coarsened with time. This was verified by observing a decrease

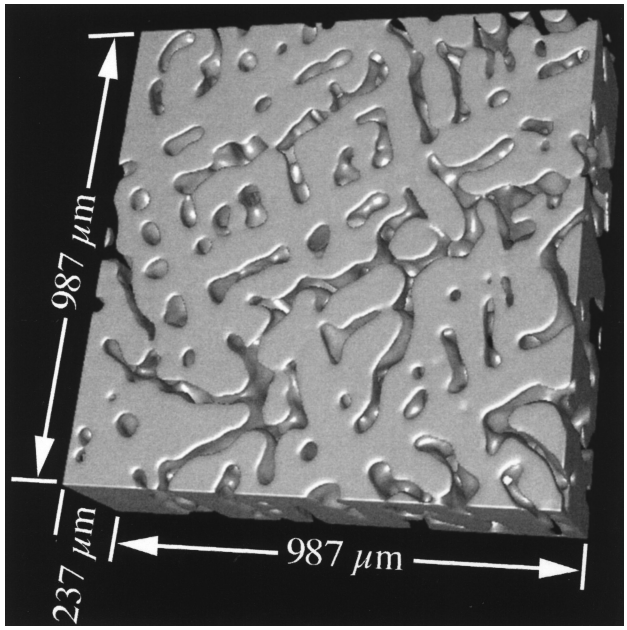

(*a*)

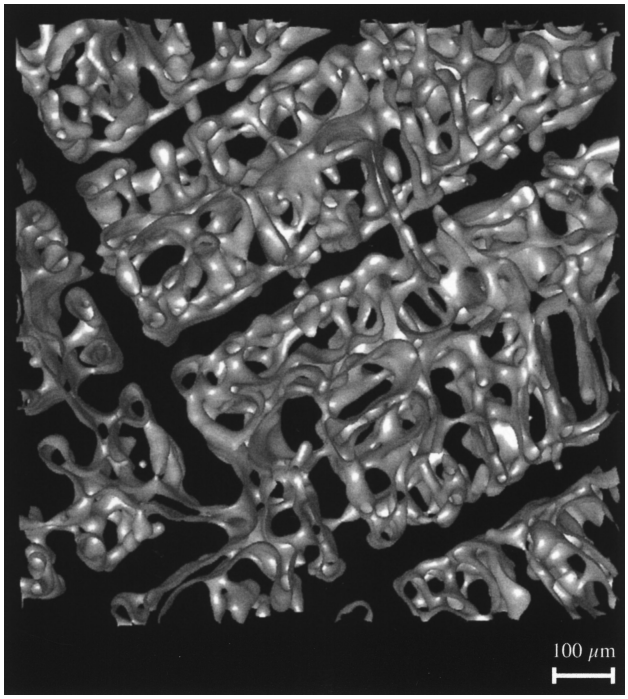

(*b*)

Fig. 12—Reconstructions of the 10-min coarsened sample are shown based on 50 serial sections taken 4.75 μm apart. (*a*) Solid denotes the aluminum dendrites, while the clear voids in the microstructure represent the liquid phase. (*b*) Only the interfaces are shown by making both the aluminum dendrites and liquid phase transparent. The growth direction is perpendicular to the top surface of (a). The view of (b) is such that one is looking along the growth direction of the sample.

in surface area per unit volume, S_v, from 24.3×10^3 [1/m] for the 10-minute sample to 9.38×10^3 [1/m] for the 964-minute sample. In the 10-minute sample, the majority of the solid and liquid phases are interconnected (Figure 12(b)). The microstructure for the 964-minute sample is also mostly interconnected, but contains multiple spherical regions composed of liquid not found in the 10-minute sample. The

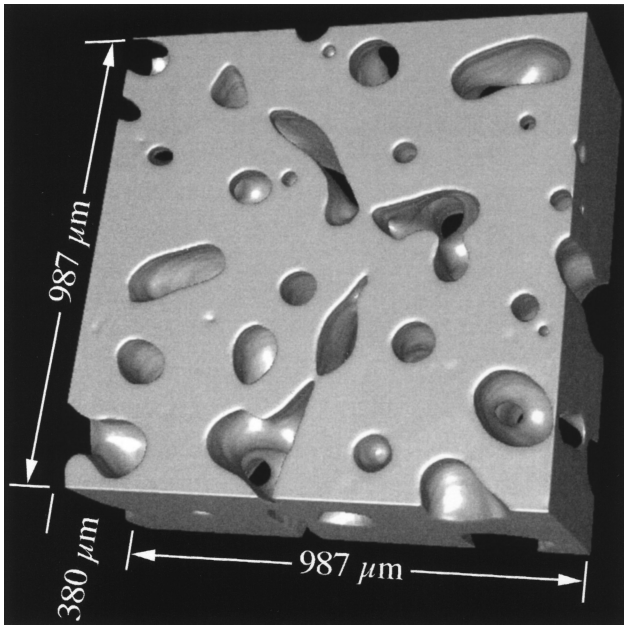

(*a*)

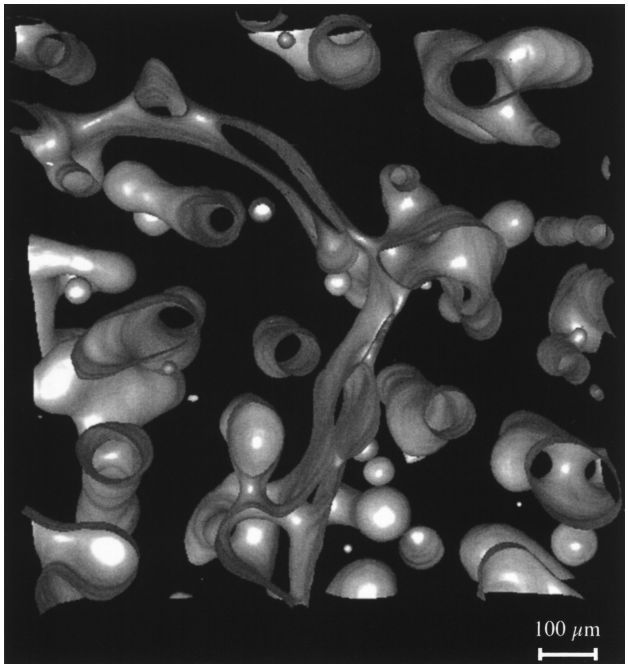

(*b*)

Fig. 13—Reconstructions of the 964-minute coarsened sample are shown based on 80 serial sections taken 4.75 μm apart. (*a*) Solid denotes the aluminum dendrites and the voids in the microstructure represent the eutectic phase. (*b*) Only the interfaces are shown by making both the aluminum dendrites and eutectic phase transparent. The growth direction is perpendicular to the top surface of (a). The view of (b) is such that one is looking down the growth direction of the sample.

microstructure for the 10-minute sample is fourfold symmetric, whereas such an anisotropy is not apparent for the 964-minute sample.

To quantitatively determine the presence of any preferential directionality of the microstructure, orientation probability density plots were generated for the microstructures (Figure 14). For both the 10-minute and the 964-minute coarsened samples, the majority of the normals of the interface are centered along the line $\theta = \pi/2$, indicating that most of the interface is parallel to the growth direction. This can be verified by examining the microstructure of the 964-minute coarsened sample (Figure 13), which contained many cylindrical and planar interfaces that are parallel to the growth direction. Although the microstructure of the 10-minute sample does not appear to have a large fraction of interface perpendicular to the growth direction, the quantitative analysis of the interfacial normals shown in Figure 14(a) clearly shows that there is a preference for the normals to be perpendicular to the growth direction.

The peaks in Figure 14 indicate the anisotropy of the microstructure. Figure 14(a) contains four peaks, which implies an approximate fourfold symmetry that is also apparent in Figure 12(b). The fourfold symmetry of the 10-minute sample is consistent with the fourfold anisotropy of the interfacial energy. Because the dendrites grow along $\langle 100 \rangle$, which is along the $\theta = 0$ direction, one would expect a fourfold symmetry in the plane perpendicular to the growth direction. A twofold symmetry is observed for the 964-minute coarsened sample (Figure 14(b)). The 964-minute coarsened sample is primarily composed of cylinders, spheres, and planar interfaces. Cylindrical and spherical interfaces would not cause peaks in orientation probability density plots; as previously mentioned, cylindrical interfaces would be represented by a line along $\theta = \pi/2$. Thus, the two peaks observed in Figure 14(b) are likely the result of the planar interfaces within the microstructure.

Figure 15 shows probability density plots of κ_1 and κ_2 for both the 10- and 964-minute coarsened samples. There is a primary peak for the 10-minute sample located near $\kappa_2 = 0.015$ [$1/\mu$m]. Since κ_1 is nearly zero, the peak corresponds to shapes that are solid cylinders. Upon coarsening, this peak moves closer to $\kappa_1 = \kappa_2$, which is consistent with an overall increase in the size scale of the microstructure. However, a second peak appears at $\kappa_1 = -0.02$ [$1/\mu$m] with κ_2 nearly zero. This corresponds to liquid cylinders, which are evident in Figure 14(b). Comparing the shapes near $\kappa_1 = \kappa_2$ between the two coarsening times reveals that solid spherical shapes ($\kappa_1 = \kappa_2 > 0$) disappeared to a greater degree then liquid spherical shapes ($\kappa_1 = \kappa_2 < 0$).

Probability density plots of the mean and Gaussian curvature are shown in Figure 16. The majority of the interfaces are saddle-shaped ($K < 0$). The larger decrease in solid spherical shapes compared to liquid spherical shapes seen in Figure 15 can also be seen in Figure 16 by examining the evolution of the probability density plots with shapes near the $H^2 - K = 0$ line. With coarsening time, the peak approaches $H = K = 0$ and the fraction of interfaces with extreme positive and negative mean and Gaussian curvatures decreased, narrowing the distribution to a region around $H = K = 0$. As previously described, deposition of material occurs at areas with large negative mean curvature, while material is removed from areas with large positive mean curvatures. Thus, the deposition and removal of material along the interface explains the decrease in mean curvatures with large absolute values observed in Figure 16.

Coarsening times between 10 and 964 minutes and larger than 964 minutes are needed to study the evolution of the microstructure in more detail. It will also be interesting to see if the trends that are observed will continue for longer

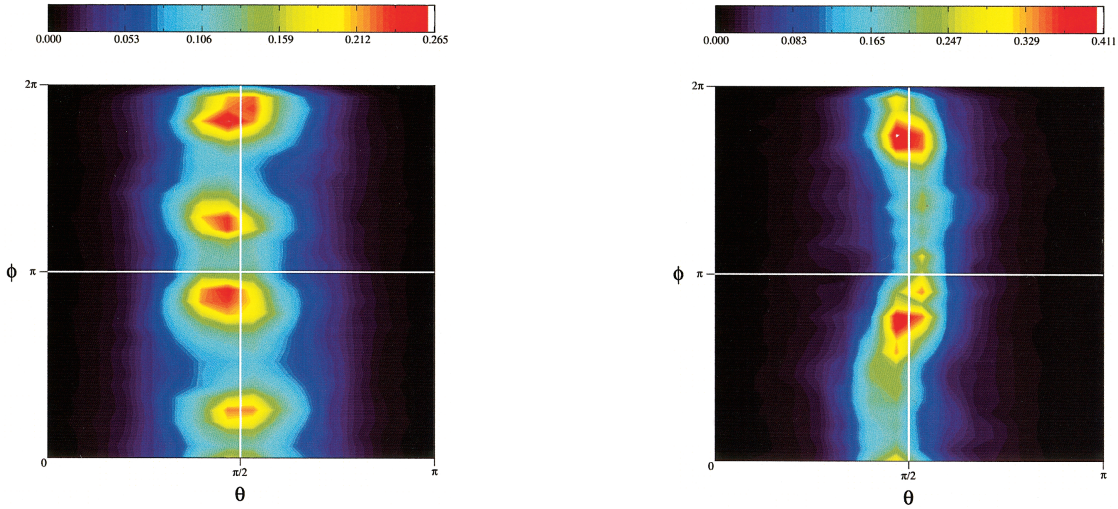

(*a*) (*b*)

Fig. 14—Probability density plots showing the orientation of the point normals to the interface for the (*a*) 10 and (*b*) 964 minute coarsened samples.

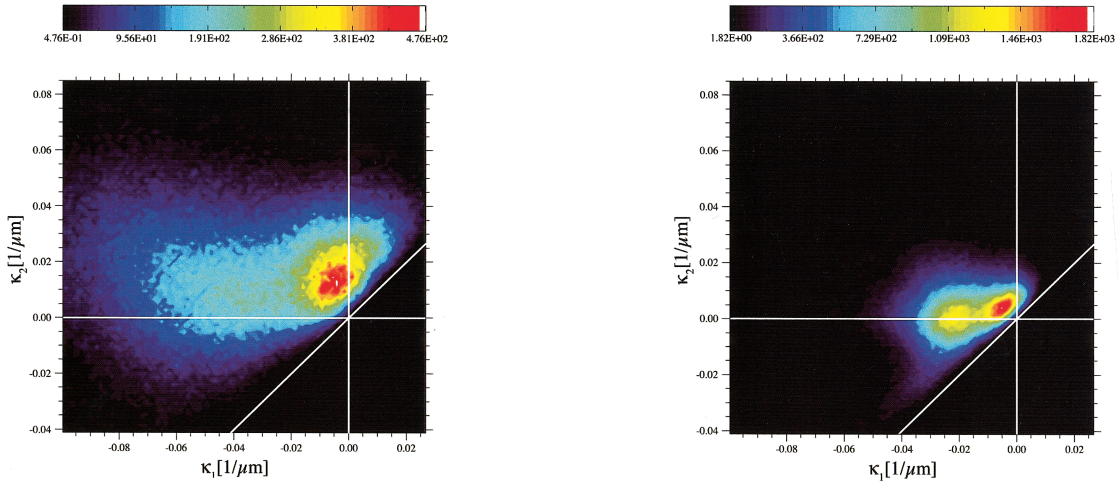

(*a*) (*b*)

Fig. 15—Probability density plots of κ_1 *vs* κ_2 for the (*a*) 10-min and (*b*) 964-min coarsened samples.

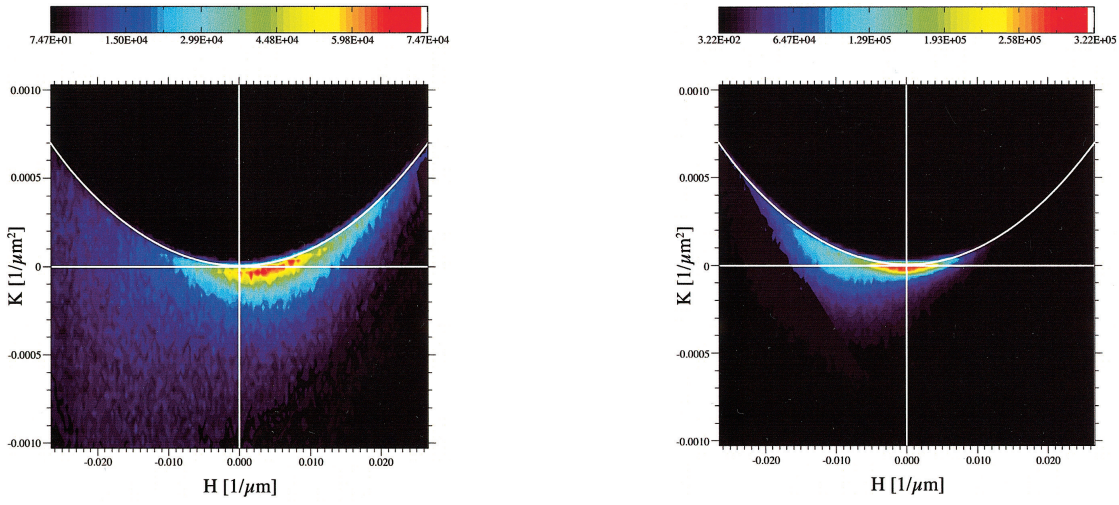

(*a*) (*b*)

Fig. 16—Probability density plots of the mean curvature and Gaussian curvature for (*a*) 10-min and (*b*) 964-min coarsened samples.

coarsening times and if the liquid cylinders that were observed for the 964-minute coarsened sample evolve to an array of spherical liquid drops.

V. CONCLUSIONS

Two Al-15 wt pct Cu dendritic samples were isothermally coarsened for 10 and 964 minutes. The surface area per unit volume was found to decrease from 24.3×10^3 [1/m] for the 10-minute sample to 9.38×10^3 [1/m] for the 964-minute sample. The three-dimensional reconstructions of the microstructures show that there are significant morphological differences between the two samples. To analyze quantitatively the microstructure, the mean and Gaussian curvatures of the interfaces were determined. *Via* a series of probability density plots, it was possible to quantify the microstructural evolution. Orientation probability density plots showed that there was a fourfold symmetry to the microstructure in the 10-minute sample, which was reduced to a twofold symmetry after coarsening for 964 minutes. However, in both samples, the majority of the interfaces were parallel with the growth direction. The probability density plots of the mean and Gaussian curvatures in conjunction with the principal curvature probability density plots revealed that there was a trend for extreme positive and negative means and Gaussian curvatures to decrease over time, that most of the interfaces were saddle-shaped, and that solid spherical shapes disappeared to a greater degree then liquid spherical shapes.

ACKNOWLEDGMENTS

The financial support from NASA, Grant No. NAG8-1660, and the Department of Energy, Grant No. DE-FG02-99ER45782, is gratefully acknowledged.

REFERENCES

1. I.M. Lifshitz and V.V. Slyozov: *J. Phys. Chem. Solids*, 1961, vol. 19, pp. 35-50.
2. C. Wagner: *Z. Elektrochem.*, 1961, vol. 65, pp. 581-91.
3. T.F. Bower, H.D. Brody, and M.C. Flemings: *Trans. TMS-AIME*, 1966, vol. 236, pp. 624-34.
4. S.P. Marsh and M.E. Glicksman: *Metall. Mater. Trans. A*, 1996, vol. 27A, 557-67.
5. T.Z. Kattamis, J.C. Coughlin, and M.C. Flemings: *Trans. TMS-AIME*, 1967, vol. 239, pp. 1504-11.
6. Manfred Kahlweit: *Scripta Metall.*, 1968, vol. 2, pp. 251-54.
7. A. Papapetrou: *Z. Kristall.*, 1935, vol. 92, pp. 89-130.
8. A.A. Chernov: *Kristallografiya*, 1956, vol. 1 (5), pp. 583-87.
9. M.O. Klia: *Kristallografiya*, 1956, vol. 65 (5), pp. 576-81.
10. K.P. Young and D.H. Kirkwood: *Metall. Trans. A*, 1975, vol. 6A, pp. 197-205.
11. S.C. Huang and M.E. Glicksman: *Acta Metall.*, 1981, vol. 29, pp. 717-34.
12. J. Alkemper and P.W. Voorhees: *J. Microsc.*, 2001, vol. 201, pp. 388-94.
13. D.A. Drew: *SIAM J. Appl. Math*, 1990, vol. 50, pp. 649-66.
14. H. Jinnai, T. Koga, Y. Nishikawa, T. Hashimoto, and S. Hyde: *Phys. Rev. Lett.*, 1997, vol. 78 (11), pp. 2248-51.
15. J. Alkemper and P.W. Voorhees: *Acta Mater.*, 2001, vol. 49, pp. 897-902.